Sains Malaysiana 46(11)(2017): 2061-2074
http://dx.doi.org/10.17576/jsm-2017-4611-06

Experimental Study on Propagation and Attenuation Regularity of Landslide Surge

(Kajian Uji Kaji ke atas Ketetapan Perambatan dan Pemerosotan Pusuan Gelongsoran Tanah)

Fuxing Zu, Pingyi Wang, Jiqing Xu & Liquan Xie*

ABSTRACT

On the basis of landslide surge model test by adopting generalized simulation of waterways, this paper, for the first time, established a four-dimensional mathematical model between wave height transmissibility rate and the initial wave height, water depth, azimuth angle as well as propagation distance through utilizing the method of tensor space mapping. Using the new model, we proposed an empirical wave field covering all areas of the channel including the attenuation area within the width of a landslide mass, the straight channel attenuation area outside the width of the landslide mass, the curved channel attenuation area and the after-curve attenuation area, which comprehensively reflects the progressive changes of surge wave factors. The transmissibility of wave height and propagation distance are in a bivariate negative exponential distribution, and the wave height gradually reduces and the attenuation also slows down as the propagation distance increases; wave height transmissibility rate, azimuth and propagation distance are in a trivariate negative exponential distribution, the attenuation of the wave height in the straight channel within the width of the landslide mass was the slowest, followed by that of wave in the straight channel outside the width of the landslide mass, and the attenuation of the wave height in the curved channel is the greatest. This empirical wave field was based on test data, scientifically abstracted the general regularity of the propagation and attenuation of landslide surge, which can be applied to similar analyses and forecasts on landslide surge and can scientifically and accurately determine the damage range of landslide surge.

Keywords: Attenuation regularity; damage range; empirical wave field; four-dimensional mathematical model; landslide surge; propagation regularity; tensor space mapping

ABSTRAK

Berdasarkan ujian model pusuan gelongsoran tanah dengan menggunakan simulasi menyeluruh laluan air, untuk pertama kali dalam kertas ini, dibangunkan sebuah model matematik empat dimensi antara kadar ketersebaran ketinggian ombak dan ketinggian gelombang pemula, kedalaman air, sudut azimuth serta jarak perambatan melalui penggunaan kaedah pemetaan ruang tensor. Menggunakan model baru ini, kami cadangkan bidang gelombang empirik meliputi semua kawasan saluran termasuk kawasan pemerosotan dalam lingkungan lebar jisim gelongsoran tanah, saluran lurus kawasan pemerosotan di luar kelebaran jisim gelongsoran tanah, saluran lengkung kawasan pemerosotan dan kawasan pemerosotan selepas lengkung, yang secara menyeluruh menunjukkan perubahan progresif faktor pusuan gelombang. Ketersebaran ketinggian ombak dan jarak perambatan adalah dalam agihan eksponen negatif bivariat serta ketinggian gelombang secara beransur-ansur berkurang dan pemerosotan juga semakin berkurang apabila jarak perambatan meningkat; kadar ketersebaran ketinggian gelombang, jarak antara azimut dan perambatan berada dalam taburan trivariat negatif eksponen, pemerosotan ketinggian ombak di saluran lurus dalam lebar jisim gelongsoran tanah adalah paling lambat, diikuti dengan ombak di saluran lurus di luar lebar jisim gelongsoran tanah dan pemerosotan ketinggian ombak di saluran lengkung adalah terbaik. Bidang gelombang empirik ini adalah berdasarkan data ujian, diabstrak secara saintifik dengan ketetapan umum perambatan dan pemerosotan pusuan gelongsoran tanah, yang boleh digunakan untuk analisis dan ramalan tentang pusuan gelongsoran tanah yang sama dan secara saintifik dan tepat menentukan julat kerosakan pusuan gelongsoran tanah.

Kata kunci: pusuan gelongsoran tanah; ketetapan perambatan; ketetapan pemerosotan, pemetaan ruang tensor; model matematik empat dimensi; bidang gelombang empirik; julat kerosakan

Introduction

Landslide is a geological disaster that can cause great damage. If land slides into rivers, lakes or seas, the landslide surge caused will lead to even greater secondary disasters, which mainly reflects into two parts: one is the disaster in areas close to the landslide mass, including the geological disasters in areas near the landslide mass and the surge disasters in nearby water areas; the other is the disaster in landslide surge propagation areas, which is caused by the propagation of landslide surge and when the surge is propagating in areas on the upper and lower reaches of the river or on the same or opposite bank of the river, it will directly threaten lives and property of people on both banks of the river, hence the damage is in a wider scope and at a more severe level. For example, the landslide happened at Vajont Reservoir in Italy (Wang 2005; Zhong 1993), the landslide in Yunyang County in the Three Gorges Reservoir area (Li & Jipazi 1988; Wang 2005), the landslide in Zigui County, Hubei Province (Xue et al. 1988; Yi et al. 2011) and the landslide on Qinggan River (Li et al. 2006) - a tributary stream of the Yangtze River, all caused huge secondary disasters due to landslide surge.

Currently, certain progress on research about landslide surge has been achieved both at home and abroad. In terms of numerical calculation analysis, Noda (1970) established a calculation formula among the initial height of landslide surge, the velocity of landslide and water depth; Rvadkiewicz et al. (1996) established a calculation model for submarine landslide surge; Heinrich et al. (1999) established a three-dimensional fluid dynamics model of surge. Panizzo et al. (2002) adopted wavelet transform method to analyze the height of the surface wave of landslide surge. Wieczorek et al. (2003) derived an empirical calculation formula for landslide surge through regression analysis. Fritz et al. (2004) conducted in-depth analysis on the two-dimensional calculation of landslide surge. Watts et al. (2005) did two-dimensional and three-dimensional calculation analysis on underwater landslide surge.

As for physical model test analysis, Kamphuis and Bowering (1971) put forward that the height of a landslide surge is determined by the volume of the landslide mass and the Froude number (Fr). Slingerland and Paolo (1982) derived an empirical formula for calculating the initial wave height and dimensionless kinetic energy. Fritz et al. (2003) studied the features of water body flow field under the effect of surge. de Carvalho (2007) analyzed the features of the pressure of surge to the wave of reservoir bank. Ataie-Ashtiani and Nik-Khah (2008) established an empirical formula between the cycle and amplitude of landslide surge. Heller et al. (2008) pointed out that the scale effect would influence the relative amplitude. Di Risio et al. (2009a) studied the regularity of wave run-up on round-shaped bank slope. The model test by Di Risio et al. (2009b) was based on videoing measures and conducted in-depth analysis and research on the three-dimensional flow field of landslide surge.

Research on landslide at channel reservoir in mountainous regions is a complicated topic that covers a wide range. Although many domestic and foreign scholars have done a large amount of research on relevant topics, their research is mainly targeted at a specific question or conducted under an ideal condition, whereas a relatively in-depth and complete theory and calculation method on the features of landslide surge in channel reservoir, particularly the regularity of the propagation and attenuation of landslide surge is still absent (Mustaffa et al. 2017). On the basis of analyzing existing materials and results, this paper conducted comprehensive test analysis and combined straight and curved sections of waterways together to systematically investigate the regularity of the propagation and attenuation of landslide surge, so as to scientifically and precisely determine the damage scope of landslide surge.

Design of general model test

Determination of model scale

According to the model similarity criterion and in order to satisfy the physical similarity between the model and the prototype, firstly similar conditions must be satisfied. This research regarded the process of land sliding into water as a whole and the process of the landslide mass moving under its own gravity should mainly consider the similarity of gravity, therefore, the model was designed based on the gravity similarity principle. Taking the mechanical conditions and operability into consideration, the geometrical scale of the physical model test about the influence of rock mass on landslide surge and shipping channels was determined as 1:70 and then various scales of the test were as follows: Geometrical scale $\lambda_l = 70$, area scale $\lambda_s = \lambda_l^2 = 70^2$, volume scale $\lambda_v = \lambda_l^3 = 70^3$, gravity scale $\lambda_g = 1$, specific gravity scale $\lambda_\sigma = 1$, speed scale $\lambda_\gamma = \sqrt{\lambda_l} = \sqrt{70}$, time scale $\lambda_t = \sqrt{\lambda_l} = \sqrt{70}$, mass scale $\lambda_m = \lambda_l^3 = 70^3$, force scale $\lambda_F = \lambda_l^3 = 70^3$, and energy scale $\lambda_E = \lambda_l^4 = 70^4$.

Design of the landslide surge model

River channel model

Channel Plane Simulation In order to make the research representative, we chose Wanzhou section in Three Gorges Reservoir Region as the prototype. This section is 6 km long, the upstream is straight and downstream is approximately 90 DEG bend. On both sides of the river terrain is tilted slopes and there are many ports. Second Wanzhou Yangtze River bridge stands at the downstream end. Zhuxi River from the left bank flows into the Yangtze River and the estuary area is silted (Anis Syuhada et al. 2016; Md Pauzi et al. 2017). General simulation was applied to straight channels and the general bending angle of curved channels was 90° and the actual land-form was adopted for the simulation of curved channels, as shown in Figures 2 and 3.

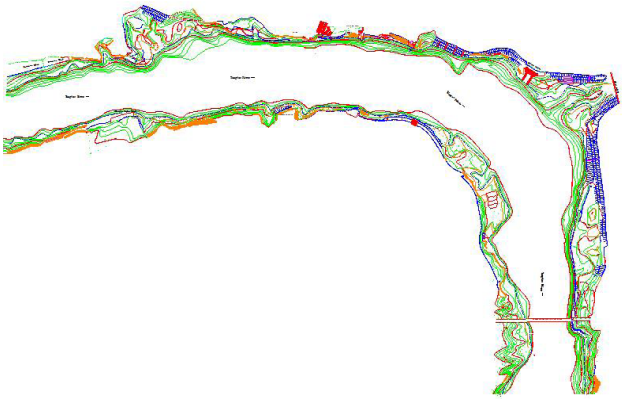

FIGURE 1. Plan graph of channel prototype

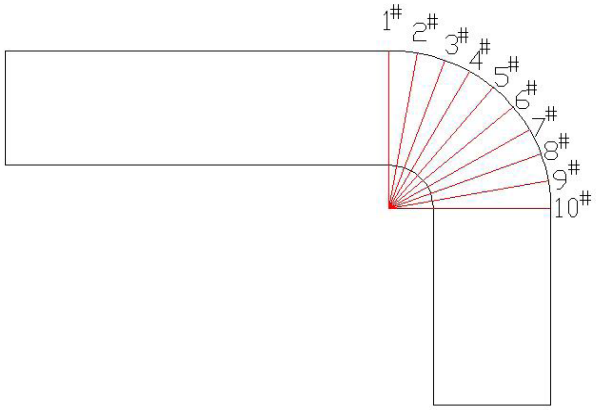

FIGURE 3. Section layout

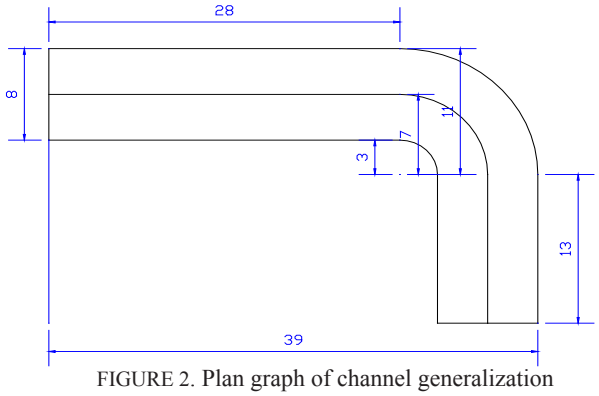

FIGURE 2. Plan graph of channel generalization (measurement: m)

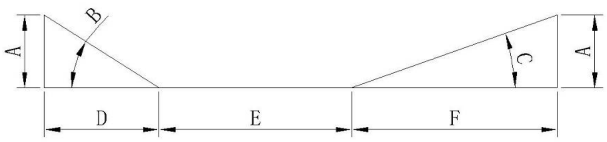

FIGURE 4. Sketch of section shape

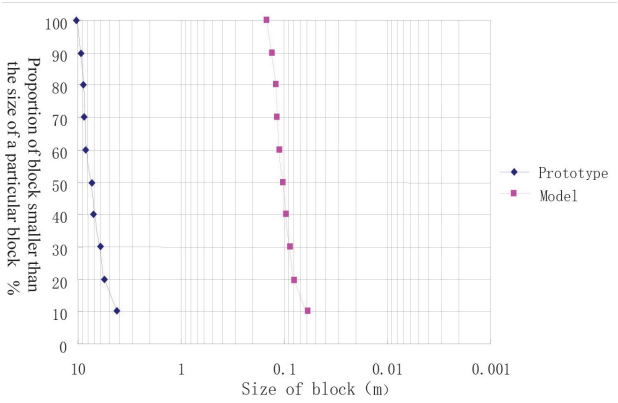

FIGURE 5. Fracture grading curve

Channel Section Simulation Select the straight and curved sections in the river. According to the section statistics shows that straight section size is consistent, the bend section size is different. Design model of the gradual way, in river bend every 10º design a section size, specific arrangement as shown in Figures 3 and 4. The specific profile data is shown in Table 1.

TABLE 1. Sectional dimension table

NO.	A(m)	B(°)	C(°)	D(m)	E(m)	F(m)
Straight section	1.16	33	20	1.79	2.94	3.27
Bend 1#	1.16	28	16	2.20	1.68	4.12
2#	1.16	32	14	1.84	1.41	4.75
3#	1.16	26	17	2.36	1.84	3.80
4#	1.16	41	18	1.35	2.96	3.69
5#	1.16	25	19	2.47	2.17	3.36
6#	1.16	28	19	2.22	2.43	3.35
7#	1.16	29	20	2.11	2.69	3.20
8#	1.16	29	18	2.14	2.27	3.59
9#	1.16	28	20	2.23	2.53	3.24
10#	1.16	28	20	2.23	2.53	3.24

TABLE 2. Table of the geometric parameters of the generalized landslide mass

Length of rock mass landslide (m)	Width of rock mass landslide (m)	Thickness of rock mass landslide (m)
1	0.5	0.2
1	1.0	0.4
1	1.5	0.6

TABLE 3. Table about the size of small blocks

Block size	Length/cm	Width/cm	Thickness/cm	Volume/cm^3	Notes
Dmax	21	14	6	1764	D60 means 60% of blocks had diameters less than such a diameter and so on.
D60	18	12	5	1080	
D40	15	10	4	600	
D20	12	8	3	288	
D10	9	6	2	108	

FIGURE 6. The landslide mass model

LANDSLIDE MASS, CHUTE AND SUPPORTIVE FRAME

Landslide Mass The volume and geometrical form of rock mass landslide determine the magnitude of its overall energy. Through statistics about the geometrical form and features of rock mass landslide in the Three Gorges Reservoir area, it has been found out that, the quantity of rock mass landslide in the reservoir area is mainly in large or middle-sized scale and in various forms. Having considered the geometric scale and the convenience of test operation, this model test generalized the rock mass slide as a cuboid, the length of the landslide mass was fixed at 1 m and its volume was controlled by the different ratios between the width and thickness of the landslide mass and combining with the statistics about the length-width ratio of landslide in the Three Gorges Reservoir area, the following three combinations of width and thickness were adopted which is shown in Table 2.

Statistics about the slope of sliding surface in rock mass landslide area in the reservoir area, it was found that, the slope was between 20-60° and the test selected three slopes, 20°, 40° and 60° as the slope of the rock mass landslide. The landslide mass in the Three Gorges Reservoir area is largely mudstone and sandstone and the natural density of sandstone is 2.2 - 2.7 g/cm^3 and that of mudstone is 2.45 - 2.65 g/cm^3. According to the density similarity principle, this test simulation took the average density of mudstone and sandstone as the density of the landslide mass. Rock landslide mass is mainly made up of rock blocks and the interspace between different structural planes (weak interlayer, fracture and fault). According to the statistics, fracture development is a phenomenon commonly existing in rock landslide mass and simulation with scattered landslide mass is more accurate than simulation with one whole landslide mass. Therefore, this test adopted small blocks of mass to do simulation based on a certain quantity ratio. Fractures are in different sizes and they are notably scattered. In order to reflect this feature accurately on the size of the mass blocks, by referencing to the diameter grading principle of sediment grain, the fractures were drew into grading curves and eigenvalues were selected from the grading curves as the basis for the geometrical size of the block (Figure 5 & Table 3).

According to the statistics about the structural fractures and the development degree in the landslide mass area in the reservoir area, the mass was divided into 5 types of small clocks, which were Dmax, D60, D40, D20 and D10 respectively and they were piled up as a whole based on the calculation and matching about the grading plans and quantity in each landslide mass plan.

FIGURE 7. The ultrasonic wave collection and analysis device

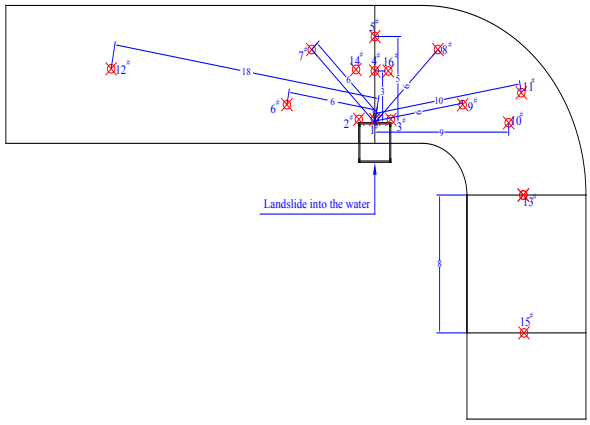

FIGURE 8. The floor plan of measuring points of landslide surge (measurement: m)

Chute Metallic materials were used to make the sliding chute, and the bottom iron plate simulated the sliding surface. The sliding chute was 2 m long. Both sides were installed with baffles with a variable range of 0.5 - 1.5 m.

LAYOUT OF MEASURING POINTS OF LANDSLIDE SURGE AS WELL AS DATA COLLECTION AND MEASUREMENT

As shown in Figure 7, the observation and measurement of wave height and cycle used the ultrasonic wave collection and analysis device.

As shown in Figure 8, there were 16 wave height measuring points. There was an ultrasonic sensor at each wave height measuring point to measure the initial surge and progressive surge. The main measuring areas included straight channel area, straight channel remote area, curved channel area and after-curve area. The data collection system mainly collected data about the wave height and cycle in different areas, and the length of collection time was normally 200 s and the collection frequency was 50 Hz.

TEST DATA ANALYSIS AND THE REGULARITY OF SURGE PROPAGATION AND ATTENUATION

DEFINITION OF RESEARCH INDEXES

After landslide surge is generated, it will propagate along different directions within the channel. During the propagation process, surge will be influenced by the shape and form of channels, water depth, internal vortex motion of water, frictional resistance, penetration and air resistance of riverbed, therefore, the wave features of progressive surge will also constantly change and attenuate (Md Pauzi et al. 2017). The propagation and attenuation of progressive surge mainly includes the propagation and attenuation of the shape and form of wave, wave height, cycle and wave steepness, and this paper took the transmissibility rate of wave height which is the most significant factor as the measuring index. The corresponding definitions are as follows: wave height transmissibility rate is the ratio between the wave height and initial wave height in corresponding positions and the highest wave height generated by landslide blocks falling into water is taken as the initial wave height, and theoretically, the position is the mid-point of the width of the front end of the landslide blocks falling into water; the relative distance is the ration between the actual distance and the initial wave height and the actual distance is the straight-line distance from the calculating point to the starting point of the initial wave height, on both curved section and straight section of the waterway; the working condition is defined by the ratio between the initial wave height and water depth and under the same working condition, the initial wave height is the same at different azimuth angles, while the initial wave height is different under different working conditions; the azimuth angle at the place right above the landslide site in Figure 8 was specified as 0 degree, and it was negative in clockwise and positive in anti-clockwise and the measurement of the azimuth angle is recorded in radians.

CLASSIFICATION OF LANDSLIDE SURGE ATTENUATION AREAS ON CURVED CHANNELS

Through test observations, the shape and form of channels and the width of landslide mass had great influence on the shape and form of wave propagation. As landslide mass becomes wider, the impact range of surge propagation will also become wider and the extent of surge attenuation will be slower (Mustaffa et al. 2017). The attenuation form and density degree of wave height contour line on the straight channel within the width of the landslide mass, the straight channel outside the width of the landslide mass, curved attenuation area and after-curve channel were all different. The plane contour map of wave of curved channel at different measuring points was drawn as Figure 9.

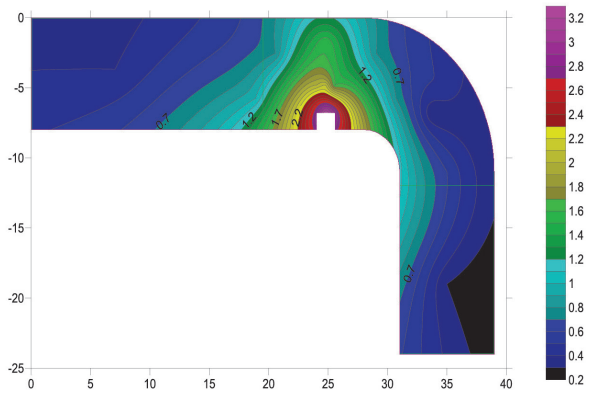

FIGURE 9. The plane contour diagram of wave height (measurement: m)

Therefore, the attenuation of wave height of progressive surge was divided into four areas based on the analysis of the contour map of wave height on curved channel, i.e. attenuation area within the width of the landslide mass (B), straight channel attenuation area outside the width of the landslide mass (A), curved channel attenuation area (C) and after-curve attenuation area (D).

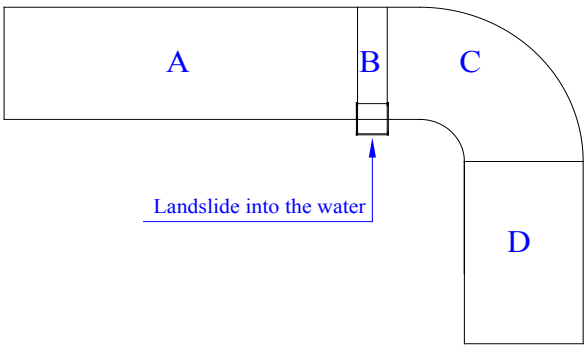

FIGURE 10. Diagram of classification of wave height attenuation areas of progressive surge

THE TWO-DIMENSIONAL MODEL BETWEEN WAVE HEIGHT TRANSMISSIBILITY RATE AND THE RELATIVE DISTANCE

By analyzing the experiment data, with given working condition and azimuth angle, Figures 11 and 12 display partial actually-measured data about the relationship between wave height transmissibility rate and the relative distance.

It can be seen from the figures that, with given working condition and azimuth angle, the progressive wave height of landslide surge gradually decreased and the attenuation gradually slowed down as the propagation distance increased, therefore, the relationship between wave height transmissibility rate and the relative distance was in a bivariate negative exponential distribution.

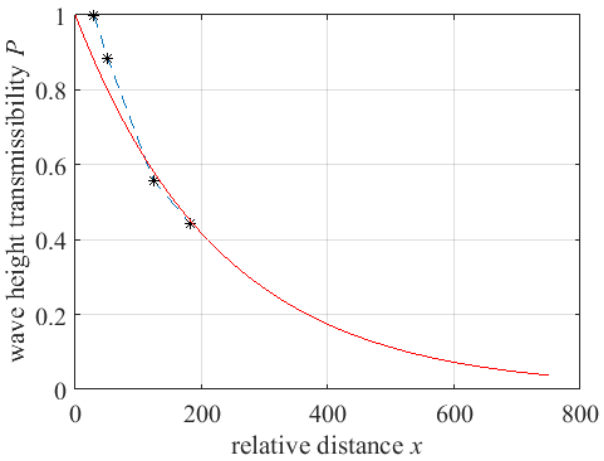

FIGURE 11. The relationship between wave height attenuation and the relative distance when the working condition was 0.0459 and azimuth angle was -0.658

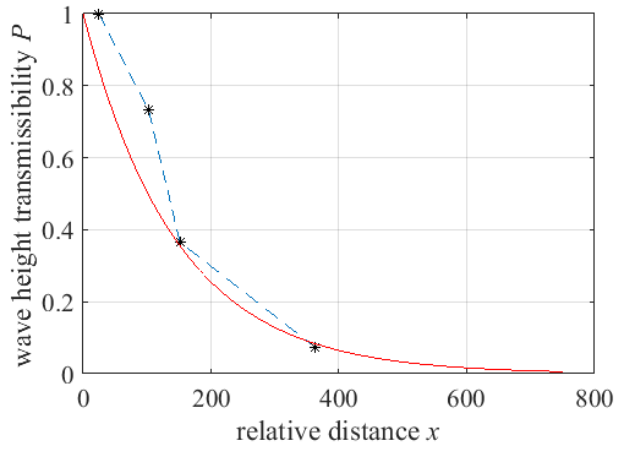

FIGURE 12. The relationship between wave height attenuation and the relative distance when the working condition was 0.0466 and azimuth angle was -2.402

THE THREE-DIMENSIONAL MODEL BETWEEN WAVE HEIGHT TRANSMISSIBILITY RATE AND THE AZIMUTH ANGLE AS WELL AS THE RELATIVE DISTANCE

Under the given working condition, Figures 13 and 14 show partial regularity of how the wave height transmissibility rate of landslide surge changed along with the changes in azimuth angle and the relative distance.

It can be seen from the diagram that, under the given working condition, the transmissibility rate displayed a negative tri-variate. At the same distance, the attenuation of wave height in the straight channel within the width of the landslide mass was the slowest, followed by that of the straight section outside the width of the landslide and the attenuation of the wave height in the curved section was the greatest. This was because during the process of the landslide mass sliding into water, near the position with

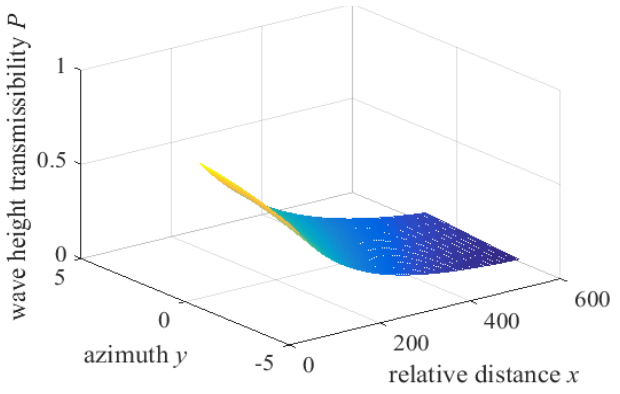

FIGURE 13. Regularity of change of wave height transmissibility rate along with the change of azimuth and relative distance when the working condition is 0.0323

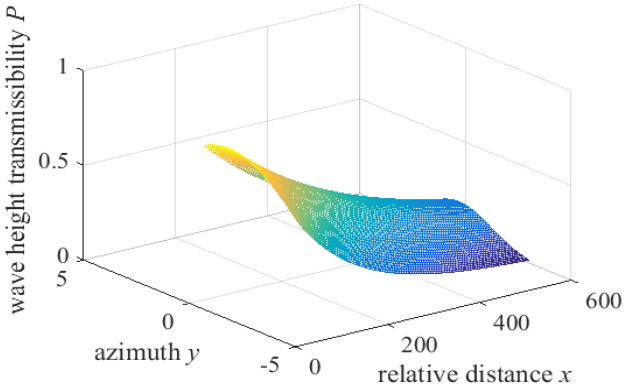

FIGURE 14. Regularity of change of wave height transmissibility rate along with the change of azimuth and relative distance when the working condition is 0.0375

0° azimuth angle directly faced by the landslide mass, the wave energy was relatively concentrated and together with the great influence of reflection stacking effect on the opposite bank (based on the test, the reflection effect on the opposite bank had more obvious influence on the stacking of wave height), therefore, its attenuation was relatively slow; while in directions deviated further from the 0° azimuth angle, wave energy was relatively scattered and its reflection influence was relatively small, therefore its wave height attenuated at a relatively fast pace (Anis Syuhada et al. 2016; Md Pauzi et al. 2017).

THE FOUR-DIMENSIONAL MODEL BETWEEN WAVE HEIGHT TRANSMISSIBILITY RATE AND WORKING CONDITION, AZIMUTH AS WELL AS THE RELATIVE DISTANCE

During the propagation process, the size of the wave height of progressive surge was affected by the initial wave height, water depth, degree of energy exchange, shape and form of river and all these factors interrelate with and influence each other. The calculation of the wave height of progressive surge is mainly conducted by studying the relationship between the wave height of progressive surge and the influence factors, hence derives the attenuation coefficient of progressive surge, and with given initial wave height, the value of the wave height can be calculated via the attenuation coefficient. In curved channels, the attenuation degree of surge wave height in different areas also varies. Therefore, the traditional idea is to determine the empirical calculation formula for the wave height of progressive surge through research and regression analysis of the influence factors, while this paper used tensor space mapping (Flugge 1972) method and took the test data as the foundation to conduct multi-factor analysis and established an empirical wave field in the straight channel within the width of the landslide mass, the straight channel outside the width of the landslide mass and the attenuation area in the curved channel, which comprehensively reflected the progressive changes of surge wave factors (in essence, it was a four-dimensional mathematical model):

$$P_k = e^{\left[\sum_{i=1}^{1}\sum_{j=1}^{3}\sum_{m=1}^{2} D_{ijm} A_i(x) B_j(y) C_m(z)\right]} .$$

P_k is the wave height transmissibility. This formula is an empirical formula calculating the value of P_k by using the tensor space mapping method and based on test data. It can be regarded as the expression of the 'tensor' and it conducts traversal summation to i=1, to j from 1~3 and to m from 1~2, respectively.

In the formula,

$$A = [x]$$
$$B = [1 \quad y \quad y^2] ,$$
$$C = [1 \quad z]$$

where x is the initial distance; y is the azimuth; z is the working condition; D_{ijm} is the component value of the three-order tensor from the perspective of tensor mapping; and it can be defined as the coefficient of a multivariate function from the perspective of function fitting. The values are as follows:

$$D_{111} = -0.7634\times10^{-3};\ D_{121} = -0.1981\times10^{-3};\ D_{131} = -0.2092\times10^{-3};$$
$$D_{112} = -0.1477;\ D_{122} = -0.0031;\ D_{132} = -0.0007; \quad .$$

The formula can be applied when the relative distance is between 100~600, the azimuth angle is between -2.4~1.3 and the working condition is between 0.015~0.260. Through calculating the value of the empirical field, the safe navigation distance of vessels can be determined.

Analyzing the experiment data according to the four-dimensional mathematical model, some of the results are shown in Tables 4 to 11 and Figure 15. Figure 15 is the four-dimensional slice map of the formula for the wave height transmissibility rate Pk and the changes in *Pk* is in correspondence with the regularity of changes in the shade of the color. Tables 4 to 11 show the wave transmissibility rates calculated by this formula with corresponding

working condition, azimuth angle and relative distance. They make it more convenient to check the value in actual engineering projects. Since the quantity of data is relatively large, only part of the results is listed here.

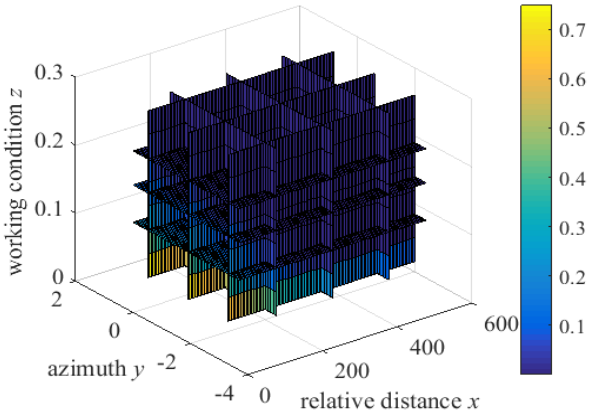

FIGURE 15. The regularity of the changes of wave height transmissibility rate along with the working condition, azimuth and the relative distance

TABLE 4. The change of the wave height transmissibility rate when the working condition is 0.015

Relative	Azimuth									
distance	-2.4	-2.3	-2.2	-2.1	-2	-1.9	-1.8	-1.7	-1.6	-1.5
100	0.6241	0.6315	0.6388	0.6458	0.6527	0.6594	0.6660	0.6723	0.6784	0.6842
105	0.6095	0.6172	0.6246	0.6319	0.6390	0.6459	0.6526	0.6590	0.6653	0.6714
110	0.5953	0.6031	0.6108	0.6182	0.6255	0.6326	0.6394	0.6461	0.6525	0.6588
115	0.5815	0.5894	0.5972	0.6048	0.6123	0.6195	0.6266	0.6334	0.6400	0.6464
120	0.5679	0.5760	0.5840	0.5918	0.5994	0.6068	0.6140	0.6209	0.6277	0.6342
125	0.5547	0.5629	0.5710	0.5790	0.5867	0.5943	0.6016	0.6087	0.6156	0.6223
130	0.5418	0.5502	0.5584	0.5664	0.5743	0.5820	0.5895	0.5968	0.6038	0.6106
135	0.5291	0.5377	0.5460	0.5542	0.5622	0.5700	0.5776	0.5850	0.5922	0.5991
140	0.5168	0.5254	0.5339	0.5422	0.5503	0.5583	0.5660	0.5735	0.5808	0.5879
145	0.5048	0.5135	0.5221	0.5305	0.5387	0.5468	0.5546	0.5623	0.5697	0.5768
150	0.4930	0.5018	0.5105	0.5190	0.5274	0.5355	0.5435	0.5512	0.5587	0.5660
155	0.4815	0.4904	0.4992	0.5078	0.5162	0.5245	0.5325	0.5404	0.5480	0.5554
160	0.4703	0.4793	0.4881	0.4968	0.5053	0.5137	0.5218	0.5297	0.5375	0.5449
165	0.4593	0.4684	0.4773	0.4861	0.4947	0.5031	0.5113	0.5193	0.5271	0.5347
170	0.4486	0.4578	0.4667	0.4756	0.4842	0.4927	0.5010	0.5091	0.5170	0.5246
175	0.4382	0.4474	0.4564	0.4653	0.4740	0.4826	0.4909	0.4991	0.5071	0.5148

TABLE 5. The change of the wave height transmissibility rate when the working condition is 0.050

Relative distance	Azimuth									
	-2.4	-2.3	-2.2	-2.1	-2	-1.9	-1.8	-1.7	-1.6	-1.5
100	0.3674	0.3718	0.3760	0.3803	0.3844	0.3884	0.3923	0.3962	0.3999	0.4035
105	0.3494	0.3538	0.3581	0.3623	0.3664	0.3705	0.3744	0.3783	0.3820	0.3856
110	0.3324	0.3367	0.3410	0.3452	0.3493	0.3534	0.3573	0.3611	0.3649	0.3685
115	0.3161	0.3205	0.3247	0.3289	0.3330	0.3370	0.3410	0.3448	0.3485	0.3522
120	0.3007	0.3050	0.3092	0.3134	0.3175	0.3215	0.3254	0.3292	0.3329	0.3365
125	0.2860	0.2903	0.2945	0.2986	0.3027	0.3066	0.3105	0.3143	0.3180	0.3216
130	0.2720	0.2763	0.2804	0.2845	0.2885	0.2925	0.2963	0.3001	0.3038	0.3074
135	0.2588	0.2629	0.2670	0.2711	0.2751	0.2790	0.2828	0.2865	0.2902	0.2937
140	0.2461	0.2502	0.2543	0.2583	0.2622	0.2661	0.2699	0.2736	0.2772	0.2807
145	0.2341	0.2382	0.2422	0.2461	0.2500	0.2538	0.2575	0.2612	0.2648	0.2682
150	0.2227	0.2267	0.2306	0.2345	0.2383	0.2421	0.2458	0.2494	0.2529	0.2563
155	0.2118	0.2157	0.2196	0.2234	0.2272	0.2309	0.2345	0.2381	0.2416	0.2450
160	0.2015	0.2053	0.2091	0.2129	0.2166	0.2202	0.2238	0.2273	0.2307	0.2341
165	0.1916	0.1954	0.1991	0.2028	0.2065	0.2101	0.2136	0.2170	0.2204	0.2237
170	0.1823	0.1860	0.1896	0.1933	0.1968	0.2004	0.2038	0.2072	0.2105	0.2138
175	0.1734	0.1770	0.1806	0.1841	0.1876	0.1911	0.1945	0.1978	0.2011	0.2043

TABLE 6. The change of the wave height transmissibility rate when the working condition is 0.085

Relative distance	Azimuth									
	-2.4	-2.3	-2.2	-2.1	-2	-1.9	-1.8	-1.7	-1.6	-1.5
100	0.2163	0.2188	0.2214	0.2239	0.2264	0.2288	0.2311	0.2335	0.2357	0.2380
105	0.2003	0.2028	0.2053	0.2077	0.2101	0.2125	0.2148	0.2171	0.2193	0.2215
110	0.1856	0.1880	0.1904	0.1928	0.1951	0.1974	0.1997	0.2019	0.2040	0.2062
115	0.1719	0.1742	0.1766	0.1789	0.1811	0.1834	0.1856	0.1877	0.1898	0.1919
120	0.1592	0.1615	0.1637	0.1660	0.1682	0.1703	0.1724	0.1745	0.1766	0.1786
125	0.1475	0.1497	0.1519	0.1540	0.1561	0.1582	0.1603	0.1623	0.1643	0.1662
130	0.1366	0.1387	0.1408	0.1429	0.1450	0.1470	0.1490	0.1509	0.1528	0.1547
135	0.1265	0.1286	0.1306	0.1326	0.1346	0.1365	0.1384	0.1403	0.1422	0.1440
140	0.1172	0.1192	0.1211	0.1230	0.1249	0.1268	0.1287	0.1305	0.1323	0.1340
145	0.1086	0.1105	0.1123	0.1142	0.1160	0.1178	0.1196	0.1213	0.1230	0.1247
150	0.1006	0.1024	0.1042	0.1059	0.1077	0.1094	0.1111	0.1128	0.1145	0.1161
155	0.0932	0.0949	0.0966	0.0983	0.1000	0.1016	0.1033	0.1049	0.1065	0.1081
160	0.0863	0.0879	0.0896	0.0912	0.0928	0.0944	0.0960	0.0975	0.0991	0.1006
165	0.0799	0.0815	0.0831	0.0846	0.0862	0.0877	0.0892	0.0907	0.0922	0.0936
170	0.0740	0.0755	0.0770	0.0785	0.0800	0.0815	0.0829	0.0843	0.0857	0.0871
175	0.0686	0.0700	0.0715	0.0729	0.0743	0.0757	0.0771	0.0784	0.0798	0.0811
180	0.0635	0.0649	0.0663	0.0676	0.0690	0.0703	0.0716	0.0729	0.0742	0.0755

TABLE 7. The change of the wave height transmissibility rate when the working condition is 0.12

Relative	Azimuth									
distance	-2.4	-2.3	-2.2	-2.1	-2	-1.9	-1.8	-1.7	-1.6	-1.5
100	0.1273	0.1288	0.1303	0.1318	0.1333	0.1347	0.1362	0.1376	0.1390	0.1403
105	0.1148	0.1163	0.1177	0.1191	0.1205	0.1219	0.1233	0.1246	0.1259	0.1272
110	0.1036	0.1050	0.1063	0.1076	0.1090	0.1103	0.1116	0.1128	0.1141	0.1153
115	0.0935	0.0947	0.0960	0.0973	0.0985	0.0998	0.1010	0.1022	0.1034	0.1045
120	0.0843	0.0855	0.0867	0.0879	0.0891	0.0902	0.0914	0.0925	0.0937	0.0948
125	0.0760	0.0772	0.0783	0.0794	0.0805	0.0816	0.0827	0.0838	0.0849	0.0859
130	0.0686	0.0697	0.0707	0.0718	0.0728	0.0739	0.0749	0.0759	0.0769	0.0779
135	0.0619	0.0629	0.0639	0.0649	0.0658	0.0668	0.0678	0.0687	0.0697	0.0706
140	0.0558	0.0568	0.0577	0.0586	0.0595	0.0604	0.0613	0.0622	0.0631	0.0640
145	0.0504	0.0512	0.0521	0.0530	0.0538	0.0547	0.0555	0.0564	0.0572	0.0580
150	0.0454	0.0462	0.0471	0.0479	0.0487	0.0495	0.0503	0.0510	0.0518	0.0526
155	0.0410	0.0417	0.0425	0.0432	0.0440	0.0447	0.0455	0.0462	0.0469	0.0477
160	0.0370	0.0377	0.0384	0.0391	0.0398	0.0405	0.0412	0.0419	0.0425	0.0432
165	0.0333	0.0340	0.0347	0.0353	0.0360	0.0366	0.0373	0.0379	0.0385	0.0392
170	0.0301	0.0307	0.0313	0.0319	0.0325	0.0331	0.0337	0.0343	0.0349	0.0355
175	0.0271	0.0277	0.0283	0.0288	0.0294	0.0300	0.0305	0.0311	0.0316	0.0322

TABLE 8. The change of the wave height transmissibility rate when the working condition is 0.155

Relative	Azimuth									
distance	-2.4	-2.3	-2.2	-2.1	-2	-1.9	-1.8	-1.7	-1.6	-1.5
100	0.0749	0.0758	0.0767	0.0776	0.0785	0.0794	0.0802	0.0811	0.0819	0.0828
105	0.0658	0.0667	0.0675	0.0683	0.0691	0.0699	0.0707	0.0715	0.0723	0.0731
110	0.0578	0.0586	0.0594	0.0601	0.0609	0.0616	0.0623	0.0631	0.0638	0.0645
115	0.0508	0.0515	0.0522	0.0529	0.0536	0.0543	0.0550	0.0556	0.0563	0.0570
120	0.0446	0.0453	0.0459	0.0466	0.0472	0.0478	0.0484	0.0491	0.0497	0.0503
125	0.0392	0.0398	0.0404	0.0410	0.0415	0.0421	0.0427	0.0433	0.0438	0.0444
130	0.0344	0.0350	0.0355	0.0361	0.0366	0.0371	0.0376	0.0382	0.0387	0.0392
135	0.0303	0.0308	0.0312	0.0317	0.0322	0.0327	0.0332	0.0337	0.0341	0.0346
140	0.0266	0.0270	0.0275	0.0279	0.0284	0.0288	0.0292	0.0297	0.0301	0.0305
145	0.0234	0.0238	0.0242	0.0246	0.0250	0.0254	0.0258	0.0262	0.0266	0.0270
150	0.0205	0.0209	0.0213	0.0216	0.0220	0.0224	0.0227	0.0231	0.0235	0.0238
155	0.0180	0.0184	0.0187	0.0190	0.0194	0.0197	0.0200	0.0204	0.0207	0.0210
160	0.0158	0.0161	0.0164	0.0167	0.0171	0.0174	0.0177	0.0180	0.0183	0.0186
165	0.0139	0.0142	0.0145	0.0147	0.0150	0.0153	0.0156	0.0158	0.0161	0.0164
170	0.0122	0.0125	0.0127	0.0130	0.0132	0.0135	0.0137	0.0140	0.0142	0.0145
175	0.0107	0.0110	0.0112	0.0114	0.0116	0.0119	0.0121	0.0123	0.0125	0.0128

TABLE 9. The change of the wave height transmissibility rate when the working condition is 0.19

Relative distance	Azimuth									
	-2.4	-2.3	-2.2	-2.1	-2	-1.9	-1.8	-1.7	-1.6	-1.5
100	0.0441	0.0446	0.0452	0.0457	0.0462	0.0467	0.0473	0.0478	0.0483	0.0488
105	0.0377	0.0382	0.0387	0.0392	0.0396	0.0401	0.0406	0.0410	0.0415	0.0420
110	0.0323	0.0327	0.0331	0.0336	0.0340	0.0344	0.0348	0.0353	0.0357	0.0361
115	0.0276	0.0280	0.0284	0.0288	0.0291	0.0295	0.0299	0.0303	0.0307	0.0310
120	0.0236	0.0240	0.0243	0.0247	0.0250	0.0253	0.0257	0.0260	0.0263	0.0267
125	0.0202	0.0205	0.0208	0.0211	0.0214	0.0217	0.0220	0.0223	0.0226	0.0229
130	0.0173	0.0176	0.0178	0.0181	0.0184	0.0186	0.0189	0.0192	0.0195	0.0197
135	0.0148	0.0150	0.0153	0.0155	0.0158	0.0160	0.0162	0.0165	0.0167	0.0170
140	0.0127	0.0129	0.0131	0.0133	0.0135	0.0137	0.0139	0.0142	0.0144	0.0146
145	0.0108	0.0110	0.0112	0.0114	0.0116	0.0118	0.0120	0.0122	0.0124	0.0125
150	0.0093	0.0094	0.0096	0.0098	0.0099	0.0101	0.0103	0.0104	0.0106	0.0108
155	0.0079	0.0081	0.0082	0.0084	0.0085	0.0087	0.0088	0.0090	0.0091	0.0093
160	0.0068	0.0069	0.0070	0.0072	0.0073	0.0074	0.0076	0.0077	0.0078	0.0080
165	0.0058	0.0059	0.0060	0.0061	0.0063	0.0064	0.0065	0.0066	0.0067	0.0069
170	0.0050	0.0051	0.0052	0.0053	0.0054	0.0055	0.0056	0.0057	0.0058	0.0059
175	0.0042	0.0043	0.0044	0.0045	0.0046	0.0047	0.0048	0.0049	0.0050	0.0051

TABLE 10. The change of the wave height transmissibility rate when the working condition is 0.225

Relative distance	Azimuth									
	-2.4	-2.3	-2.2	-2.1	-2	-1.9	-1.8	-1.7	-1.6	-1.5
100	0.0260	0.0263	0.0266	0.0269	0.0272	0.0275	0.0278	0.0282	0.0285	0.0288
105	0.0216	0.0219	0.0222	0.0225	0.0227	0.0230	0.0233	0.0236	0.0238	0.0241
110	0.0180	0.0183	0.0185	0.0187	0.0190	0.0192	0.0195	0.0197	0.0199	0.0202
115	0.0150	0.0152	0.0154	0.0156	0.0159	0.0161	0.0163	0.0165	0.0167	0.0169
120	0.0125	0.0127	0.0129	0.0131	0.0132	0.0134	0.0136	0.0138	0.0140	0.0142
125	0.0104	0.0106	0.0107	0.0109	0.0111	0.0112	0.0114	0.0115	0.0117	0.0119
130	0.0087	0.0088	0.0090	0.0091	0.0092	0.0094	0.0095	0.0096	0.0098	0.0099
135	0.0072	0.0074	0.0075	0.0076	0.0077	0.0078	0.0080	0.0081	0.0082	0.0083
140	0.0060	0.0061	0.0062	0.0063	0.0064	0.0065	0.0066	0.0068	0.0069	0.0070
145	0.0050	0.0051	0.0052	0.0053	0.0054	0.0055	0.0056	0.0056	0.0057	0.0058
150	0.0042	0.0043	0.0043	0.0044	0.0045	0.0046	0.0046	0.0047	0.0048	0.0049
155	0.0035	0.0036	0.0036	0.0037	0.0038	0.0038	0.0039	0.0040	0.0040	0.0041
160	0.0029	0.0030	0.0030	0.0031	0.0031	0.0032	0.0032	0.0033	0.0034	0.0034
165	0.0024	0.0025	0.0025	0.0026	0.0026	0.0027	0.0027	0.0028	0.0028	0.0029
170	0.0020	0.0021	0.0021	0.0021	0.0022	0.0022	0.0023	0.0023	0.0024	0.0024
175	0.0017	0.0017	0.0018	0.0018	0.0018	0.0019	0.0019	0.0019	0.0020	0.0020

TABLE 11. The change of the wave height transmissibility rate when the working condition is 0.26

Relative distance	Azimuth									
	-2.4	-2.3	-2.2	-2.1	-2	-1.9	-1.8	-1.7	-1.6	-1.5
100	0.0153	0.0155	0.0157	0.0158	0.0160	0.0162	0.0164	0.0166	0.0168	0.0170
105	0.0124	0.0126	0.0127	0.0129	0.0130	0.0132	0.0134	0.0135	0.0137	0.0138
110	0.0101	0.0102	0.0103	0.0105	0.0106	0.0107	0.0109	0.0110	0.0112	0.0113
115	0.0082	0.0083	0.0084	0.0085	0.0086	0.0087	0.0089	0.0090	0.0091	0.0092
120	0.0066	0.0067	0.0068	0.0069	0.0070	0.0071	0.0072	0.0073	0.0074	0.0075
125	0.0054	0.0055	0.0055	0.0056	0.0057	0.0058	0.0059	0.0060	0.0060	0.0061
130	0.0044	0.0044	0.0045	0.0046	0.0046	0.0047	0.0048	0.0049	0.0049	0.0050
135	0.0035	0.0036	0.0037	0.0037	0.0038	0.0038	0.0039	0.0040	0.0040	0.0041
140	0.0029	0.0029	0.0030	0.0030	0.0031	0.0031	0.0032	0.0032	0.0033	0.0033
145	0.0023	0.0024	0.0024	0.0025	0.0025	0.0025	0.0026	0.0026	0.0027	0.0027
150	0.0019	0.0019	0.0020	0.0020	0.0020	0.0021	0.0021	0.0021	0.0022	0.0022
155	0.0015	0.0016	0.0016	0.0016	0.0017	0.0017	0.0017	0.0017	0.0018	0.0018
160	0.0012	0.0013	0.0013	0.0013	0.0013	0.0014	0.0014	0.0014	0.0014	0.0015
165	0.0010	0.0010	0.0011	0.0011	0.0011	0.0011	0.0011	0.0012	0.0012	0.0012
170	0.0008	0.0008	0.0009	0.0009	0.0009	0.0009	0.0009	0.0009	0.0010	0.0010
175	0.0007	0.0007	0.0007	0.0007	0.0007	0.0007	0.0008	0.0008	0.0008	0.0008

Conclusion

This paper took the typical sections of a river as the prototype, adopted general simulation method to conduct test on landslide surge model. Through analyzing the wave height contour map of curved section of the river, the attenuation of the wave height of progressive surge was classified into four areas including the attenuation area within the width of the landslide mass, the straight channel attenuation area outside the width of the landslide mass, curved channel attenuation area and after-curve attenuation area. On the basis of analysis about test data, this paper defined related indexes and parameters including the wave height transmissibility rate (the ratio between the wave height and the initial wave height in corresponding positions), the relative distance (the ratio between the actual distance and the initial wave height), azimuth angle, working condition (the ration between the initial wave height and water depth) and established a two-dimensional model between wave height transmissibility rate and the relative distance, a three-dimensional model between wave height transmissibility rate and azimuth as well as the relative distance, and a four-dimensional model between wave height transmissibility rate and the initial wave height, water depth, azimuth as well as the relative distance and explored the regularity of propagation and attenuation of landslide surge.

According to the two-dimensional model between wave height transmissibility rate and the relative distance, it was concluded that, under given working condition and azimuth angle, the progressive wave height of landslide surge gradually decreased and the attenuation gradually slowed down as the propagation distance increased, and the relationship between wage height transmissibility rate and the relative distance was in a bivariate negative exponential distribution.

Based on the three-dimensional model between wave height transmissibility rate and azimuth as well as the relative distance, it could be found that: with given working condition, the wave height transmissibility rate along with the changes in azimuth and the relative distance was in a trivariate negative exponential distribution. When the distance was the same, the attenuation of wave height in the straight channel within the width of the landslide mass was the slowest, followed by that in the straight channel outside the landslide mass, and the attenuation of wave height in the curved channel was the greatest.

This paper for the first time used tensor space mapping method to establish a four-dimensional model between wave height transmissibility rate and the initial wave height, water depth, azimuth angle as well as the relative distance and formed an empirical wave field that covered all the four areas of a river including the attenuation area within the width of the landslide mass, the straight channel attenuation area outside the width of the landslide mass, curved channel attenuation area and after-curve attenuation area, which comprehensively reflected the progressive changes of landslide surge factors. Although this empirical wave field was based on the data of this test, it can be completely abstracted from the specific test and used for analysis and forecast of other landslide surge, so as to accurately determine the damage scope of landslide surge in a scientific way.

ACKNOWLEDGEMENTS

This work is supported in part by the National Science Foundation Council under Grants 51479015 and 11172213.

REFERENCES

Anis Syuhada Mohd Saidi, Sarani Zakaria, Chin Hua Chia, Sharifah Nabihah Syed Jaafar & Farah Nadia Mohammad Padzil. 2016. Physico-mechanical properties of kenaf pulp cellulose membrane cross-linked with glyoxa. *Sains Malaysiana* 45(2): 263-270.

Ataie-Ashtiani, B. & Nik-Khah, A. 2008. Impulsive waves caused by subaerial landslides. *Journal of the Environ. Fluid Mech.* 8(7): 263-280.

de Carvalho, R.F. 2007. Landslides into reservoirs and their impacts on banks. *Journal of the Environ. Fluid Mech.* 7(2): 481-493.

Di Riso, M., De Girolamo, P., Bellotti, G., Panizzo, A., Aristodemo, F., Molfetta, M.G. & Petrillo, A.F. 2009a. Landslide-generated tsunamis runup at the coast of a conical island: New physical model experiments. *Journal of Geophysical Research* 114(C1): doi. 10.1029/2008JC004858.

Di Riso, M., Bellotti, G. & Panizzo, A. 2009b. Three-dimensional experiments on landslide generated waves at a sloping coast. *Coastal Engineering* 56: 659-667.

Flugge, W. 1972. *Tensor Analysis and Continuum Mechanics*. New York: Springer-Verlag.

Fritz, H.M., Hager, W.H. & Minor, H.E. 2004. Near field characteristics of landslide generated impulse waves. *Journal of the Waterway Port Coastal and Ocean Division, ASCE* 130(6): 287-302.

Fritz, H.M., Hager, W.H. & Minor, H.E. 2003. Landslide generated impulse waves. 1. Instantaneous flow fields. *Journal of the Experiments in Fluids* 35(l): 505-519.

Heinrich, R., Guibourge, S., Mangeney, A. & Roche, R. 1999. Numerical modeling of a landslide-generated tsunami following a potential explosion of the Montserrat volcano. *Phys. Chem. Earth (A)* 24(2): 163-168.

Heller, V., Hager, W.H. & Minor, H.E. 2008. Seale effects in subaerial landslide generated impulse waves. *Experiments in Fluids* 44(5): 691-703.

Kamphuis, J.W. & Bowering, R.J. 1971. Impulse waves generated by landslides. *ASCE, Proceedings of the 12th Coastal Engineering Conference.* 1: 689-699.

Li, H.Z., Pan, Y.Z., Wang, T.L., et al., 2006. Analysis on the causes and mechanism of Qianjiangping landslide in the Three Gorges Reservoir area. *Yangtze River* 37(7): 12-14.

Li Yusheng, Jipazi 1988. Landslide - A real case of reactivation of an old landslide in the Three Gorges area of the Yangtze River. Beijing: Science Press. pp. 323-328.

Md Pauzi Abdullah, Syafinaz Salleh, Rahmah Elfithri, Mazlin bin Mokhtar, Mohd Ekhwan Toriman, Ahmad Fuad Embi, Khairul Nizam Abdul Maulud, Maimon Abdullah, Lee Yook Heng, Syamimi Halimshah, Maizura Maizan & Nurlina Mohamad Ramzan. 2017. Stakeholders' response and perspectives on flood disaster of Pahang river basin. *Malaysian Journal of Geoscience* 1(1): 43-49.

Mustaffa Kamal Shuib, Mohammad Abdul Manap, Felix Tongkul, Ismail Bin Abd Rahim, Tajul Anuar Jamaludin, Noraini Surip, Rabieahtul Abu Bakar, Mohd Rozaidi Che Abas, Roziah Che Musa & Zahid Ahmad. 2017. Active faults in Peninsular Malaysia with emphasis on active geomorphic features of Bukit Tinggi region. *Malaysian Journal of Geoscience.* 1(1): 13-26.

Noda, E. 1970. Water waves generated by landslides. *Journal of the Waterways, Harbors and Coastal Engineering Division* 96(4): 835-855.

Panizzo, A., Bellotti, G. & De Girolamo, P. 2002. Application of wavelet transform analysis to landslide generated waves. *Coastal Engineering* 44: 321-338.

Rvadkiewicz, S.A., Marietti, C. & Heinrieh, P. 1996. Modelling of submarine landslides and generated water waves. *Phys. Chem. Earth* 21(12): 7-12.

Slingerland, R. & Paolo, B.V. 1982. Evaluating hazard of landslide-induced water waves. *Journal of the Waterway Port Coastal and Ocean Division* 108(4): 504-512.

Wang Yang. 2005. *Research on Reservoir Bank Landslide Velocity and Its Surge Disaster*. China University of Geosciences.

Watts, P., Grilli, S.T., Tappin, D.R. & Fryer, G.J. 2005. Tsunami generation by submarine mass failure. II: Predictive equations and case studies. *Journal of the Waterway Port Coastal and Ocean Division, ASCE* 131(6): 298-310.

Wiezorek, G.F., Matthias, J., Motyka, R.J., Zirnheld, S.L. & Craw, P. 2003. *Preliminary Assessment of Landslide-induced Wave Hazards: Tidal Inlet, Glacier Bay National Park, Alaska*. U.S. Geological Survey Open-File Report 03-100: U.S. Department of the Interior and U.S. Geological Survey.

Xue, G., Guifang, L.V. & Jiang, R. 1988. Research on Xintan landslide, typical landslide in China. Beijing: Science Press. pp. 200-210.

Yi, W., Meng, Z.P. & Yi, Q.L. 2011. Theory and method of forecasting landslide in the Three Gorges Reservoir area. Beijing: Science Press.

Zhong, L. 1993. Implications of the landslide in Vajont Reservoir, Italy. *The Chinese Journal of Geological Hazard and Control* 5(2): 77-84.

Fuxing Zu, Pingyi Wang & Jiqing Xu
School of River and Ocean Engineering
Chongqing Jiaotong University, Chongqing 400074
China

Liquan Xie*
Department of Hydraulic Engineering
Tongji University, Shanghai 200092
China

*Corresponding author; email: xie_liquan@tongji.edu.cn

Received: 10 January 2017
Accepted: 16 May 2017